RESEARCH PAPER

Finite element analysis of a FSMA microgripper for determination of force experienced by it due to photo induced micro actuation effect

Abhishek Bagchi[1,2] · Amalendu Biswas[3] · Gurdeep Singh[1] · Susenjit Sarkar[2] · P. K. Mukhopadhyay[1]

Abstract

In this work, we have proposed a new method to remotely control and operate the working mechanism of a suitable Ferromagnetic Shape Memory Alloy (FSMA) microactuator system using only a focused low powered laser beam. Model of a simple microgripper system fabricated from a FSMA material and operated by applying the newly discovered Photo Induced Micro Actuation (PIMA) property of FSMAs has been proposed in this report. The design of the fabricated FSMA microgripper was developed using a standard Computer Aided Engineering (CAE) software. The operating mechanism of the newly modelled microgripper assembly was thoroughly characterized numerically with Finite Element Analysis (FEA) method using the CAE software. A prototype of the microgripper system, as designed in the CAE software numerically, was fabricated and its working mechanism controlled by the PIMA effect was systematically studied. The main advantage of using this laser actuated microgripper system is the reduction in weight of the gripper assembly due to the absence of either electrical motors along with other electrical accessories or complex hydraulics systems as used in conventional gripper systems to control the working mechanism of the gripper end effectors. The gripping mechanism of the prototype microgripper system can be controlled only by the low powered laser beams. This is the first system attempted in the world where the PIMA effect was employed in any kind of microactuator application.

Keywords Ferromagnetic Shape Memory Alloys · Photo Induced Micro Actuation · Finite Element Analysis · Microactuator · Microgripper

1 Introduction

The conventional microactuators and other micro electro-mechanical systems (MEMS) used in various engineering applications are bulky as well as heavy due to the presence of complex electro-mechanical control mechanisms. To overcome these drawbacks, efforts are being made to make these systems lighter by reducing the weights of the control mechanisms [1–3]. One such alternative that has been studied extensively in recent times is the use of ferromagnetic shape memory alloys (FSMA) in the fabrication and

✉ Abhishek Bagchi
  tonybagchi@gmail.com

[1] TRC, S. N. Bose National Centre for Basic Sciences, Kolkata 700106, India

[2] Department of Mechanical Engineering, Jadavpur University, Kolkata 700032, India

[3] Department of Mechanical Engineering, Heritage Institute of Technology, Kolkata 700107, India

operation of suitable microactuators [4–6]. FSMAs have been used as the sensing and actuating materials in various MEMS and microactuators due to their ability to generate mechanical work by virtue of their shape recovery property under the influence of thermal or magnetic stimuli [7–9]. Meanwhile, a hitherto unknown phenomenon of Photo Induced Micro Actuation (PIMA) effect was discovered when a low powered focused laser beam was incident on a Co-Ni-Al FSMA metglass ribbon [10]. By virtue of this PIMA property, the FSMA systems respond to the incident laser beam by moving towards or away from the incident beam. Only FSMAs were found to have this unique property, no other material showed this effect. This laser induced actuation or PIMA effect in FSMAs is found to be rapid and fatigue resistant over millions of oscillations [10]. The discovery of the PIMA effect opened a new horizon in the fabrication and operation of suitable microactuator systems for carrying out various engineering applications.

It has already been established in earlier studies that this PIMA effect is dependent on various factors like optical

power of incident laser beam, laser polarization angle, colour or wavelength of the incident laser, apart from dependence on material composition as well as ambient temperature [10, 11]. It was also shown that the amplitude of actuation of the Co-Ni-Al ribbons could be effectively controlled by governing the various factors mentioned above [11]. Before actual implementation of this unique phenomenon in operating suitably fabricated microactuator systems is done, investigations have also been carried out to determine the workability of the Co-Ni-Al FSMA system in various environmental conditions where it was subjected to different levels of temperature and oxidation [12, 13]. The limiting functionality of PIMA property shown by the Co-Ni-Al alloy at elevated temperatures and in ambient atmosphere was determined by these studies. Limited oxidation kinetics studies of the sample also showed that this alloy is comparatively oxidation resistant with respect to other Co and Ni based alloys, with a moderate oxidation rate constant value. Previous microstructural studies of the present alloy system confirm the presence of Body Centred Cubic (BCC) based B2 ordering of the grains embedded in Face Centred Cubic (FCC) matrix channel having $L1_2$ ordering [12, 13]. It has been already established earlier that the B2 phase structure of the selected alloy gradually degraded by virtue of different heat treatment scenarios which in turn progressively reduced and eventually destroyed the PIMA property of the alloy completely. Simultaneously, it was also reported that the $L1_2$ ordered matrix channel phase was not affected by similar heat treatment procedures and it was able to retain its microstructural features. Hence, it was qualitatively concluded that the B2 phase which is the active phase responsible for the FSMA property of the alloy is also responsible for the unique PIMA property. The direct quantitative explanation of the cause of the PIMA property shown by FSMAs are yet to be discovered but the results obtained from all these studies paved the way for successful implementation of a new class of laser controlled remotely operated microactuator systems.

In this study, a new method has been proposed to achieve a remote operation and control of a FSMA microactuator utilizing this PIMA phenomenon, used as a microgripper that can grip small objects. Various microgripper systems have been designed and fabricated in the recent past according to specific requirements and are being extensively used in the field of diverse scientific and engineering applications [14–17]. The main advantages of these MEMS based microgripper systems are their compact size and low cost of production [15]. The main application areas of these microgrippers are in the field of micro assembly especially microchip assembly. Specialized microgrippers are employed to manipulate fragile biological objects etc. The working principle of these microgrippers are based on different actuation principles. The most widely used microgripper systems are based on the following principles

namely: hydraulic, pneumatic, electromagnetic, thermoelectric as well as electrostatic. The basic working principle of these microgripper systems is to grip and hold onto objects for as long as desired and then also to release the objects at the correct place and time. These microgripper systems can also be attached to robotic arms to carry out their work [18]. As mentioned before, the main disadvantage of these conventional microgrippers are that they are bulky and heavy due to the presence of either electrical motors along with other electrical accessories or complex hydraulics systems employed to control the working mechanism of the gripper end effectors. Moreover, the requirement of sensor systems for the proper operation of these microgrippers make the overall systems bulkier, heavier as well as more complex. In order to overcome these drawbacks, recently smart materials are being used in the fabrication and operation of microgripper systems. The most widely used smart materials in this field are piezoelectric materials as well as shape memory alloys. The main advantage of using smart materials is because the material itself can act both as sensor and actuator, thus making the system more compact as well as less complex. Conventional FSMA microactuators developed till now are either temperature driven or are operated by an applied magnetic field. The main disadvantage of temperature driven FSMA microactuators are their slow response time. Magnetically driven microactuators are fast to response but the presence of bulky electromagnets to control the microactuation makes the overall system heavy and complex. Therein lies the main novelty of the PIMA operated FSMA microactuators. As reported earlier, only a focused and low powered laser beam is used to control the entire sensing as well as actuation mechanism. This makes the overall system highly compact and lightweight. The control system of the PIMA operated microactuators specifically the microgripper system reported here eliminates the need of sensors and transducers of any kind making the system impervious to radio interference of any sort, thus making the system discreet. The proposed system is also suitable for operation in various radioactive as well as bio hazardous environments due to the uniqueness of the system. A very simple design of a microgripper is proposed here so as to implement the PIMA effect to control the gripping operation by only a laser light beam. The operation and controlled actuation mechanism of the fabricated FSMA microgripper model was systematically studied by three different coloured laser light sources as reported earlier [11–13].

2 Experimental and simulation details

An ingot of nominal composition $Co_{34}Ni_{35}Al_{31}$ (in atomic wt. %) alloy was prepared by arc melting the 99.99% pure constituent elements under a continuously flowing argon atmosphere in an arc melting furnace. The ribbons were

prepared from the as prepared alloy ingot by RF induction melt spinning furnace in argon atmosphere. The rotation speed of the water chilled copper wheel of the melt spinning furnace was set at 600 rpm to produce the ribbons of required thickness. The compositional analysis of the sample was carried out by a FEI made QUANTA FEG 250 model scanning electron microscope (SEM) instrument with an energy dispersive X-ray analysis (EDAX) attachment to confirm the final composition of the melt-spun ribbons. It was reported earlier [13] that the selected sample is ferromagnetic in nature at room temperature. The martensitic start and finish temperatures of the B2 ordered phase are 205 K and 130 K, while the austenitic start and finish temperatures are 215 K and 310 K respectively. It was also reported that the selected sample is ferromagnetic at room temperature having a Curie Temperature (T_C) of 365 K for the B2 structured granular phase and T_C of 1045 K for the $L1_2$ structured matrix channel.

The perceived microgripper was made from a small portion of ribbon as the sensing and actuating part of the gripper system. Other ordinary materials were used to complete the device. It was then operated by utilizing the PIMA property of the sensing and actuating parts of the device made from the FSMA parts. The opening and closing operation of the microgripper, employing different controlling mechanisms were recorded using a Nikon made Eclipse Ti-U model dual deck inverted research microscope along with its associated software. One of the decks was used to attach the halogen lamp housing for illuminating the sample through the objective lenses. The second deck of the microscope was used to simultaneously focus the laser beam onto the sample through the objective lenses along with the light source. Half mirrors were used in both the tiers of the dual deck structure for passing of light as well as laser in both directions to stimulate the sample as well as capture the image in the camera attached with the microscope for imaging purposes. The basic working principle of the dual deck microscope system is shown schematically in Fig. 1. Three different laser beams were used for detailed characterization of the device operation having wavelength of 450 nm for the blue, 532 nm for the green and 655 nm for the red laser respectively. The maximum optical power output of the laser beams incident on the FSMA sample through the microscope setup was regulated upto 95 mW for calibration with earlier actuation data [11–13].

In order to obtain the mechanical properties of the materials, nanoindentation testing was employed [20]. The indentation studies were performed using a Hysitron Inc. made TI 950 model TriboIndentor with a load range of 5 mN to 300 mN with a resolution of < 1 mN employing a Berkovich diamond indenter tip.
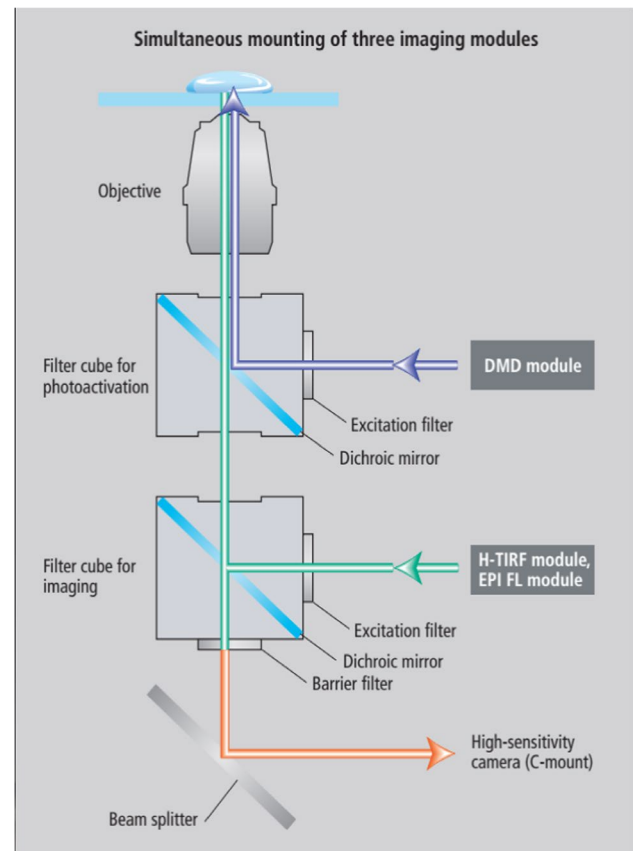

Fig. 1 Schematic representation of dual deck microscope operation [19]

Designing of PIMA operated actuation of the microgripper was done with a CAE software named ANSYS 2020R1 in its Workbench module. Both solid modeling as well as numerical analysis using Finite Element Method have been performed in ANSYS Workbench. As there is no dedicated software for numerical analysis for PIMA actuated FSMA microstructures, ANSYS was used for its designing process. This whole designing process were executed with 'Static Structural' tool in Workbench module. First, a 3-dimensional model of the microgripper was created in Design-Modeler environment, then a fine mesh was created on this model. This meshed model was simulated numerically with different static loads and corresponding deflection values were recorded. To do this simulation effectively, proper boundary conditions and contact parameters were imposed. The deflection data obtained from the simulation was calibrated against the experimental PIMA data. Thus, the correlation between the forces exerted by the focused laser beam on the selected FSMA microactuators can be inferred from the applied simulated force.

3 Results and discussions

3.1 Design of the microgripper system

The design of a microgripper system is shown schematically in Fig. 2(a). From the figure it can be seen that the prototype microgripper system consists of three parts. Part 'A' of the microgripper is the main actuating part of the assembly. Here the actuating part was fabricated

from $Co_{34}Ni_{35}Al_{31}$ ribbon. Part 'B' is the right arm of the microgripper system as seen from the front in Fig. 2(a), where aluminium was chosen as the material of construction. The left arm of the assembly was made as a duplicate of the right arm. The detailed manufacturing drawing has been shown below in Fig. 2(b).

These suitably shaped two arms were attached to the FSMA actuator as shown in Fig. 2(b). The FSMA actuator was attached to the portion 'd' of the two arms by using an

Fig. 2 a: Schematic representation of the FSMA microgripper system. Part A is the FSMA actuating part and Part B is the microgripper arm. (**b**): Detailed manufacturing drawing of the FSMA microgripper system

(a)

(b)
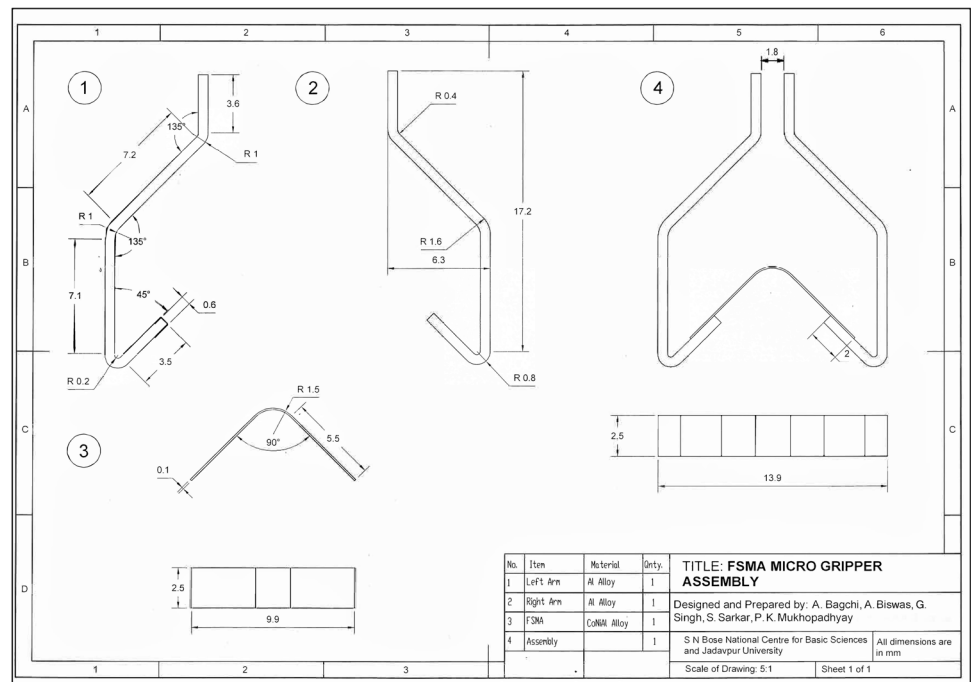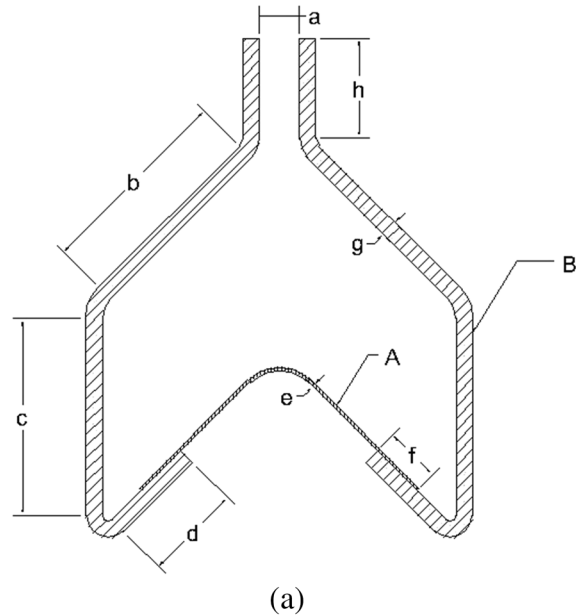
adhesive. The FSMA actuator and the two aluminium arms were overlapped by a portion 'f' as shown in the figure. The length of the overlapping between the FSMA material and the arms i.e. the dimension 'f' was approximately 2 mm. The gap between the end effectors of the two arms was approximately 1.8 mm. The actual sample which acted as both the sensor and actuator of the fabricated microgripper assembly is shown in Fig. 3(a). Similarly, one of the two identical aluminium arms which were attached to the FSMA ribbon is shown in Fig. 3(b). The finished microgripper prototype is shown in Fig. 3(c). These parts were engineered according to the dimensions mentioned above.

3.2 Working principle of the microgripper system

As described in the previous section, the prototype microgripper assembly is made up of three parts, viz. the FSMA actuator and the two aluminium arms. To operate this microgripper system, one side of the assembly was kept fixed by attaching it to a fixed support. The other arm of the microgripper assembly was kept free for actuation. This was the rest state or open state of the microgripper system when the FSMA sample was not excited by any laser beam. The microgripper assembly in this open state was positioned in the path of the incoming laser beam from the laser diode sources in such a way that the light fell directly on the "V" shaped bend of part A of the assembly. When the laser beam was turned on, the FSMA material actuated. Due to this actuation, the "V" shaped gap opened up, thus closing the gripping part of the assembly. This whole action took only 0.4 s to achieve. The microgripper assembly remained in its closed state as long as the laser beam was incident on the FSMA actuator. As soon as the laser beam was switched off, the FSMA material reverted to its original quiescent position, opening the jaw. The closing action of the FSMA material took 0.6 s to revert back to its initial state which resulted in the opening of the microgripper jaw. These opening and closing operations were found to be fatigue resistant i.e. the efficiency of closing and opening actions of the microgripper does not depend on the number of ON – OFF operations of the incident laser beam. The amplitude of actuation of the gripping mechanism as well as the closing and opening time of the microgripper arm remained the same for millions of operation cycle. Hence, it can be inferred that the gripper mechanism will be able to close its grip and hold onto any suitable object for as long as required and then it will also be able to release its grip on the object when it is deemed necessary. This is the simple operating principle followed for the operation and control of the proposed prototype microgripper system. In real-life applications, the
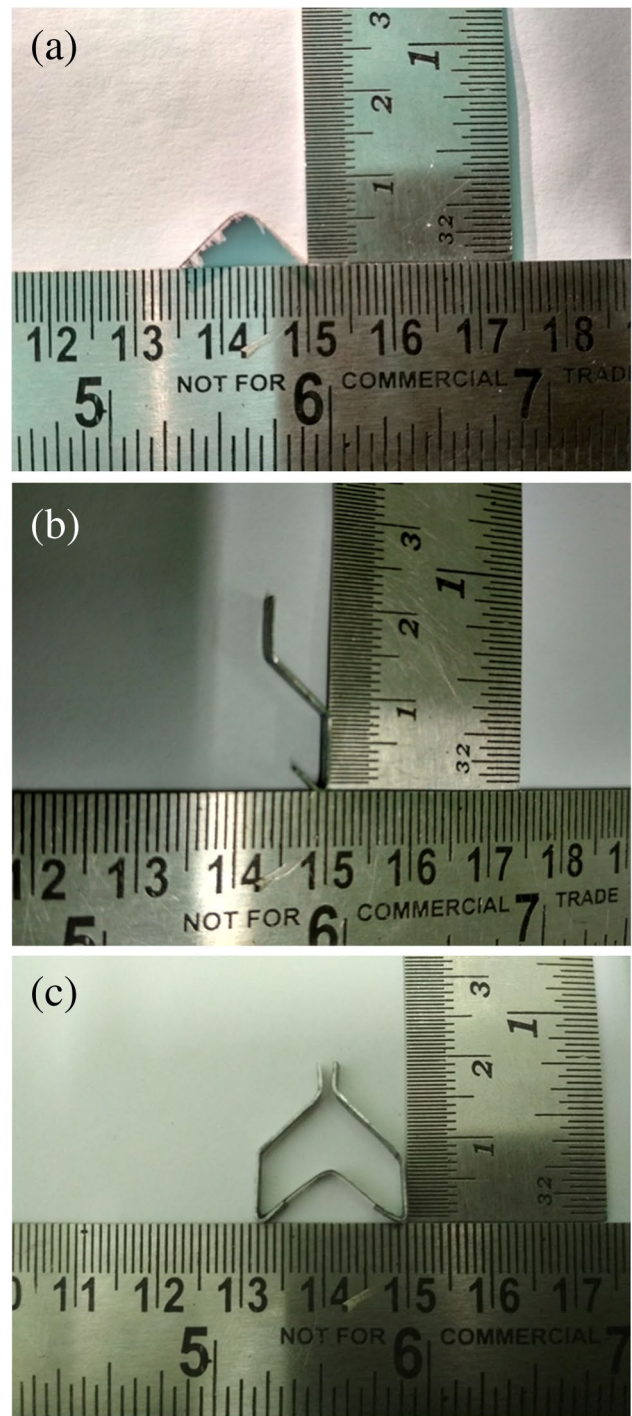

Fig. 3 a: Actuating part of FSMA microgripper system. (**b**): Gripping arm of FSMA microgripper system. (**c**): Complete prototype FSMA microgripper system assembly

developed microgripper prototype will be attached to the end of a suitable robotic arm as its end effector. The laser beam will pass through fiber optic cables running along

the robotic arm in such a way that the focused laser can be incident onto the FSMA surface remotely. As mentioned earlier in Section 1, the PIMA operated microgripper prototype can have various real-life applications. It can be envisioned being used in the micro assembly line of chip manufacturing business. Due to its uniqueness and remote controllability, it can also be used discreetly as well as in various hazardous environments. The opening and closing mechanisms of the microgripper system was observed by an optical microscope system and are shown here in Fig. 4(a-b).

3.3 Mechanical properties of the FSMA

Due to very small thickness of the melt spun FSMA ribbons as compared to their length and breadth, mechanical properties of these ribbon samples will alter significantly from the bulk samples of the same composition [21, 22]. The qualitative trend of the yield strength and ductility of these ribbons were obtained earlier from the engineering stress vs. engineering strain plots under tension at room temperature [23]. Nanoindentation studies are commonly applied to determine the elastic modulus as well as the hardness of the thin materials like the metglass alloy ribbons investigated in the present work. A typical Nanoindentation plot using a Berkovich indenter measures the continuous variation of indentation load with respect to the indenter penetration depth on the sample. From the load – displacement curve, various mechanical properties like elastic modulus, stiffness, plastic resistance and indentation hardness of the sample can be determined [24].

The indentation load vs. penetration depth plot of the sample at room temperature is shown in Fig. 5. The results obtained from analysis of the graph show that the FSMA exhibits a hardness of 121 MPa and yield strength of 40 MPa. The elastic modulus of the present sample was determined to be 15 GPa and a Poisson's ratio of 0.32. These
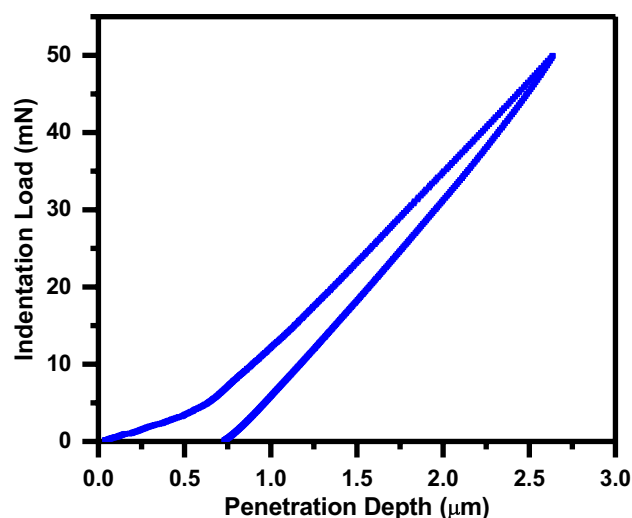
Fig. 5 Indentation load vs. penetration depth plot at room temperature of the $Co_{34}Ni_{35}Al_{31}$ FSMA system

data hint at the qualitative trend in the mechanical properties of the sample. With the help of these parameters, the $Co_{34}Ni_{35}Al_{31}$ alloy can be added as a new material to the material library of the ANSYS software.

3.4 Finite element analysis of simulated microgripper

In the present work the Gripper Model has been simulated numerically using a FEA software ANSYS 2020R1 to predict the deflection of the arm of the gripper under the action of force which the FSMA experiences when a laser beam is imposed on it. In the pre-processing steps of this FEA simulation using ANSYS Workbench 2020R1, material properties of all the parts of the Gripper have been assigned, CAD model of the gripper has been imported as an IGES file, Meshing done, Boundary Conditions and Loading imposed.

Fig. 4 **a**: Microgripper assembly in open position, (**b**): Microgripper assembly in closed position
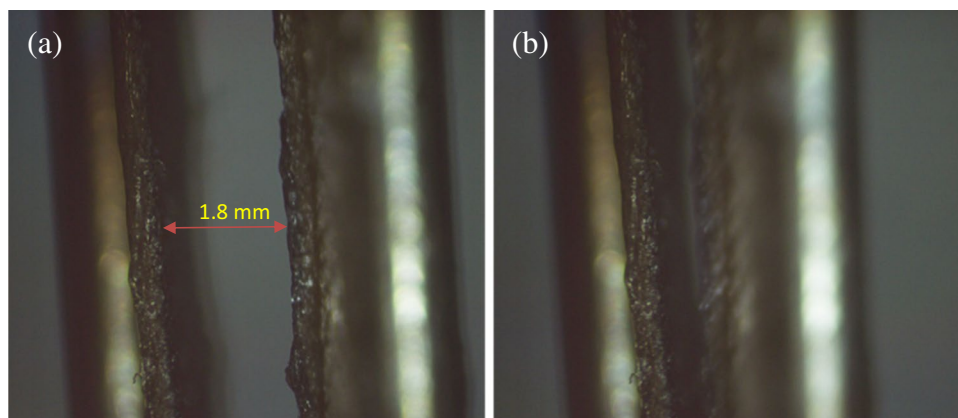
Simulation parameters controlled for the fine tuning of the results. Following are the detailed discussion on different parameters of the pre-processing step of the simulation.

3.4.1 Material Properties

The gripper model consists of two arms and one Ferromagnetic strip which works as a connector between two arms to facilitate one to move freely with respect to another. The arms are made of aluminium whose mechanical properties have been mentioned below. As discussed above, material of the strip is a newly developed ferromagnetic alloy material which has a shape memory characteristic. Different mechanical properties of this FSMA were given in a previous work [23] through different testing like tensile testing using Universal Testing Machine (UTM), nanoindentation studies etc. These mechanical properties have also been mentioned below in Table 1 (a-b).

3.4.2 3D model and its Meshing

To predict numerically the force required for the predefined deformation due to imposition of a laser beam on the strip made of this FSMA using a FEA software, a model has been constructed in a CAD software which has been presented below in Fig. 6.

In the above figure, label 'A' represents the FSMA strip. The parts labeled as 'B' and 'C' are the gripper arms made of aluminum material.

After importing IGES file of the gripper model from CAD software to the FEA software it has been meshed with hexahedral elements and in this meshing 'Fine' option of the 'Quality' parameter was chosen for proper meshing. The meshed view of the gripper assembly is shown in Fig. 7.
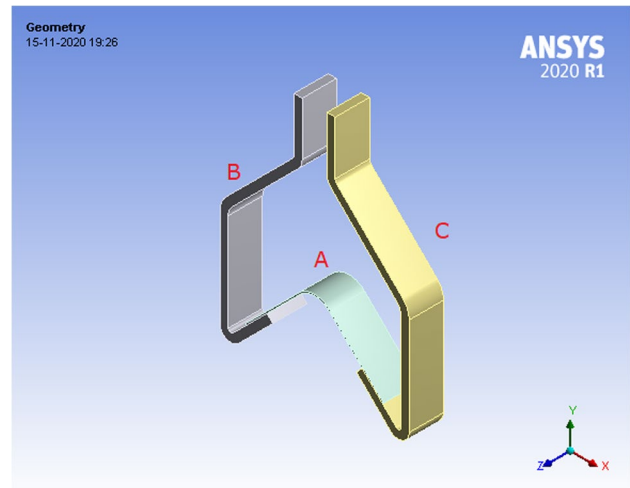

Fig. 6 CAD model of the FSMA gripper

3.4.3 Boundary conditions and Loading

The FSMA strip has been made fixed with the Aluminium arms of the gripper using 'Bonded' type of 'Contact' parameter. Among the two arms one has been kept fixed and other is free to move which has been connected with fixed arm by 'Frictional' option of the 'Contact' parameter so that when the free arm deflects can exerts pressure upon coming in contact with the fixed arm. Following is the Fig. 8, depicting all the contacts as explained above.

One arm of the gripper has been kept fixed to impose boundary conditions in accordance with the physical testing condition in lab. Here a load has been applied at the concave portion of the strip in the FEA simulation because, in the lab condition a laser beam was imposed at the concave portion

Table 1 Mechanical properties of Aluminium and $CO_{34}Ni_{35}Al_{31}$ FSMA

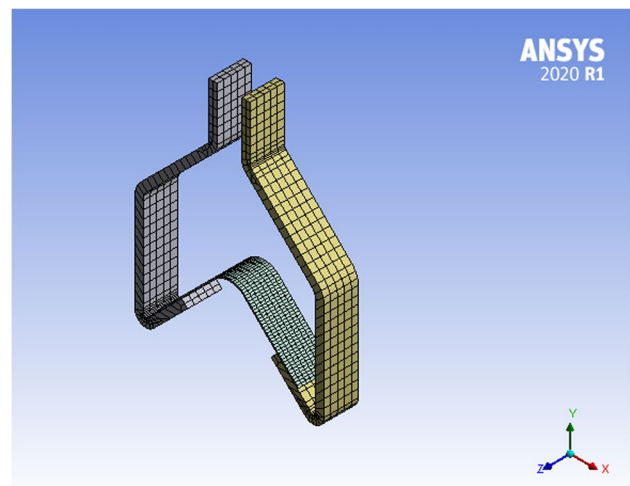| Sl No	Property description	Value	Unit
(a): Mechanical properties of aluminium			
1	Density	2700	Kg/m^3
2	Young's Modulus	70000	MPa
3	Poisson's ratio	0.28	
4	Bulk Modulus	64800	MPa
5	Shear Modulus	26515	MPa
6	Yield Strength	310	MPa
(b): Mechanical properties of FSMA material ($Co_{34}Ni_{35}Al_{31}$)			
1	Density	5029.61	Kg/m^3
2	Young's Modulus	15000	MPa
3	Poisson's ratio	0.32	
4	Bulk Modulus	13889	MPa
5	Shear Modulus	56818	MPa
6	Yield Strength	40	MPa

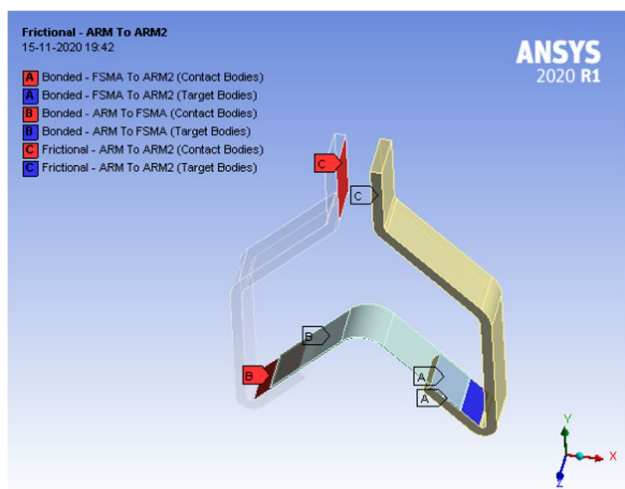**Fig. 7** Meshed view of the FSMA gripper

Fig. 8 Various contacts used in the FEA model of the Gripper with FSMA strip

of the strip. Loading and Boundary Condition have been shown in the Fig. 9 below.

3.4.4 Simulation and optimization

In the present work, FEA simulation has been used to predict the force which might be experienced by the FSMA strip attached in the gripper due to imposition of different color laser beam. To achieve this objective, deflections of the gripper arm have been determined under a range of loads from 0.06 N to 0.005 N with an interval of 0.005 N for 0.06 N to 0.01 N and with an interval of 0.001 N for 0.01 to 0.005 N. Directional deflection of the gripper arm have been determined along the normal direction of the gripper's
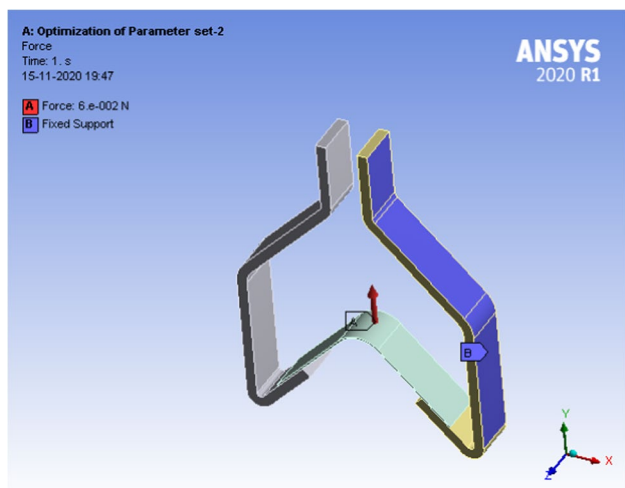

Fig. 9 Boundary condition and Loading used in the simulation

holding-end numerically using FEA software for the above mentioned forces. To do this simulation 'Large Deflection' parameter was kept on in the 'Simulation' settings. The directional deflections for the above-mentioned loads or forces are presented below in Table 2 and also in graphical form in Fig. 10.

With help of the above design points, an optimization has been performed in ANSYS using the 'Response Surface Methodology' to predict the forces that the FSMA strip might be experiencing due to imposition of different colored LASER beam on the FSMA strip. The deflection values have been determined from experiments conducted in lab using the Nikon made Eclipse Ti-U model dual deck inverted research microscope along with its associated software, where deflections against three colored LASER beam, Red, Blue and Green, of various power values were imposed on a FSMA strip of the gripper and corresponding deflections were noted down. Following is the Table 3, containing

Table 2 Design points for the directional deflections under various forces

Design Points	Force in N	Directional Deflections of the Gripper Arm in mm
DP 0 (Current)	0.06	2.203
DP 1	0.055	2.032
DP 2	0.05	1.862
DP 3	0.045	1.685
DP 4	0.04	1.505
DP 5	0.035	1.325
DP 6	0.03	1.142
DP 7	0.025	0.957
DP 8	0.02	0.769
DP 9	0.015	0.580
DP 10	0.01	0.389
DP 11	0.009	0.350
DP 12	0.008	0.311
DP 13	0.007	0.273
DP 14	0.006	0.234
DP 15	0.005	0.196
DP 16	0.004	0.157
DP 17	0.003	0.118
DP 18	0.002	0.078
DP 19	0.001	0.039
DP 20	0.0009	0.035
DP 21	0.0008	0.031
DP 22	0.0007	0.027
DP 23	0.0006	0.023
DP 24	0.0005	0.019
DP 25	0.015375	0.594
DP 26	0.045125	1.689
DP 27	0.03025	1.151
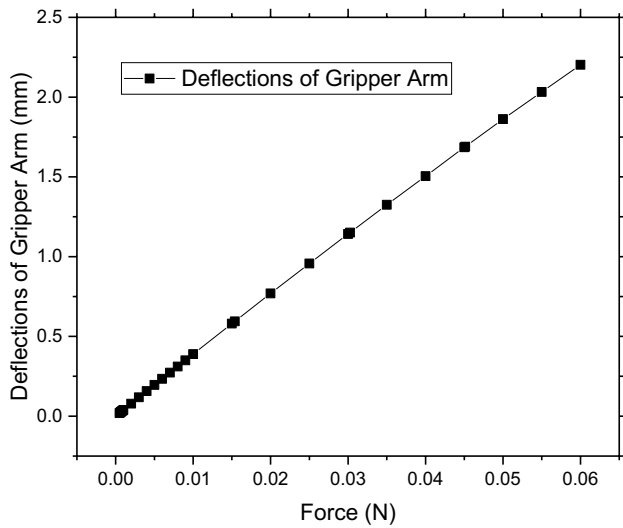
Fig. 10 Directional deflections under various forces

Fig. 11 Gripper arm deflection vs laser optical power

experimental values of deflections of gripper arm end due to imposition of various colored LASER beam of different power on the FSMA strip. The data is also presented in graphical form in Fig. 11.

Now using the design points as mentioned in the Table 2 an optimization model has been created in ANSYS with help of 'Response Surface Methodology'. In this optimization
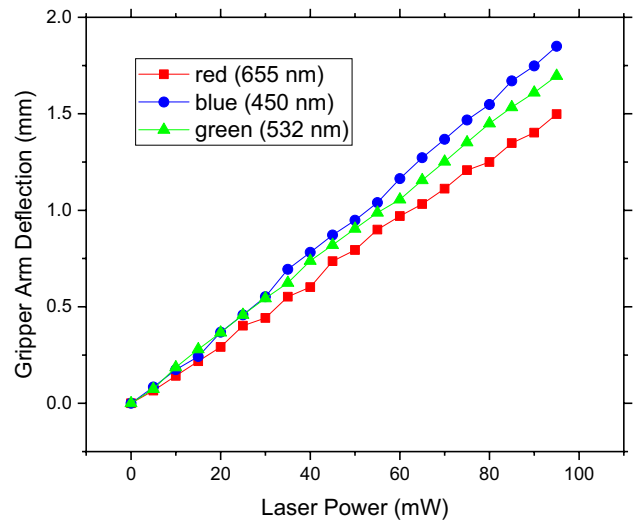
different target value have been set as per the requirement and corresponding force value has been determined.

3.5 Laser force calculation and Discussions

To find out force experienced by the FSMA strip in the gripper due to imposition of different colored Laser beam of various power, target values of gripper-end directional deflection values have been taken from Table 3 above. For each

Table 3 Experimental values of deflections due to different Laser

Power in mW	Displacement in mm due to Red Laser (655 nm)	Displacement in mm due to Blue Laser (450 nm)	Displacement in mm due to Green Laser (532 mm)
0	0	0	0
5	0.066	0.084	0.074
10	0.142	0.174	0.186
15	0.218	0.242	0.28
20	0.292	0.368	0.366
25	0.402	0.458	0.458
30	0.442	0.552	0.544
35	0.552	0.694	0.624
40	0.602	0.782	0.738
45	0.736	0.872	0.82
50	0.794	0.948	0.904
55	0.9	1.04	0.988
60	0.97	1.164	1.056
65	1.032	1.272	1.156
70	1.112	1.368	1.252
75	1.208	1.468	1.352
80	1.25	1.548	1.45
85	1.348	1.67	1.534
90	1.402	1.748	1.61
95	1.498	1.85	1.696

Table 4 Force exerted by different coloured lasers on FSMA strip

Power	Displacement	Force (Predicted by Optimization using ANSYS)	
mW	mm	mN (millinewton)	gm (gm force)
(a): Force exerted by Red Laser of wavelength 655 nm with various wattage values			
0	0	0	0
5	0.066	1.7	0.17
10	0.142	3.6	0.37
15	0.218	5.6	0.57
20	0.292	7.5	0.76
25	0.402	10.3	1.05
30	0.442	11.4	1.16
35	0.552	14.2	1.45
40	0.602	15.5	1.58
45	0.736	19.1	1.95
50	0.794	20.6	2.1
55	0.9	23.5	2.39
60	0.97	25.4	2.59
65	1.032	27	2.75
70	1.112	29.2	2.98
75	1.208	31.8	3.24
80	1.25	33	3.36
85	1.348	35.6	3.63
90	1.402	37.2	3.79
95	1.4989	39.8	4.06
(b): Force exerted by Blue Laser of wavelength 450 nm with various wattage values.			
0	0	0	0
5	0.084	2.1	0.22
10	0.174	4.4	0.45
15	0.242	6.2	0.63
20	0.368	9.5	0.97
25	0.458	11.8	1.2
30	0.552	14.4	1.47
35	0.694	18	1.83
40	0.782	20.3	2.07
45	0.872	22.7	2.31
50	0.948	24.7	2.52
55	1.04	27.2	2.77
60	1.164	30.6	3.12
65	1.272	33.6	3.42

Table 4 (continued)

Power	Displacement	Force (Predicted by Optimization using ANSYS)	
mW	mm	mN (millinewton)	gm (gm force)
70	1.368	36.2	3.69
75	1.468	39	3.97
80	1.548	41.2	4.2
85	1.67	44.6	4.54
90	1.748	46.8	4.77
95	1.8	48.3	4.92
(c): Force exerted by Green Laser of wavelength 532 nm with various wattage values			
0	0	0	0
5	0.074	1.9	0.19
10	0.186	4.8	0.49
15	0.28	7.2	0.74
20	0.366	9.4	0.96
25	0.458	11.8	1.2
30	0.544	14.3	1.46
35	0.624	16.1	1.64
40	0.738	19.1	1.95
45	0.82	21.4	2.18
50	0.904	23.6	2.41
55	0.988	25.8	2.63
60	1.056	27.6	2.82
65	1.156	30.3	3.09
70	1.252	33	3.37
75	1.352	35.7	3.64
80	1.45	38.5	3.92
85	1.534	41	4.18
90	1.61	42.9	4.38
95	1.696	45.3	4.62

target value the optimization model in ANSYS predicts the force at the concave part of the FSMA strip as shown in Fig. 9. Following Tables 4(a-c) show the values of forces the FSMA strip in the gripper would be experiencing when a laser of particular color and particular wattage is imposed on the FSMA strip causing the directional deflections of the
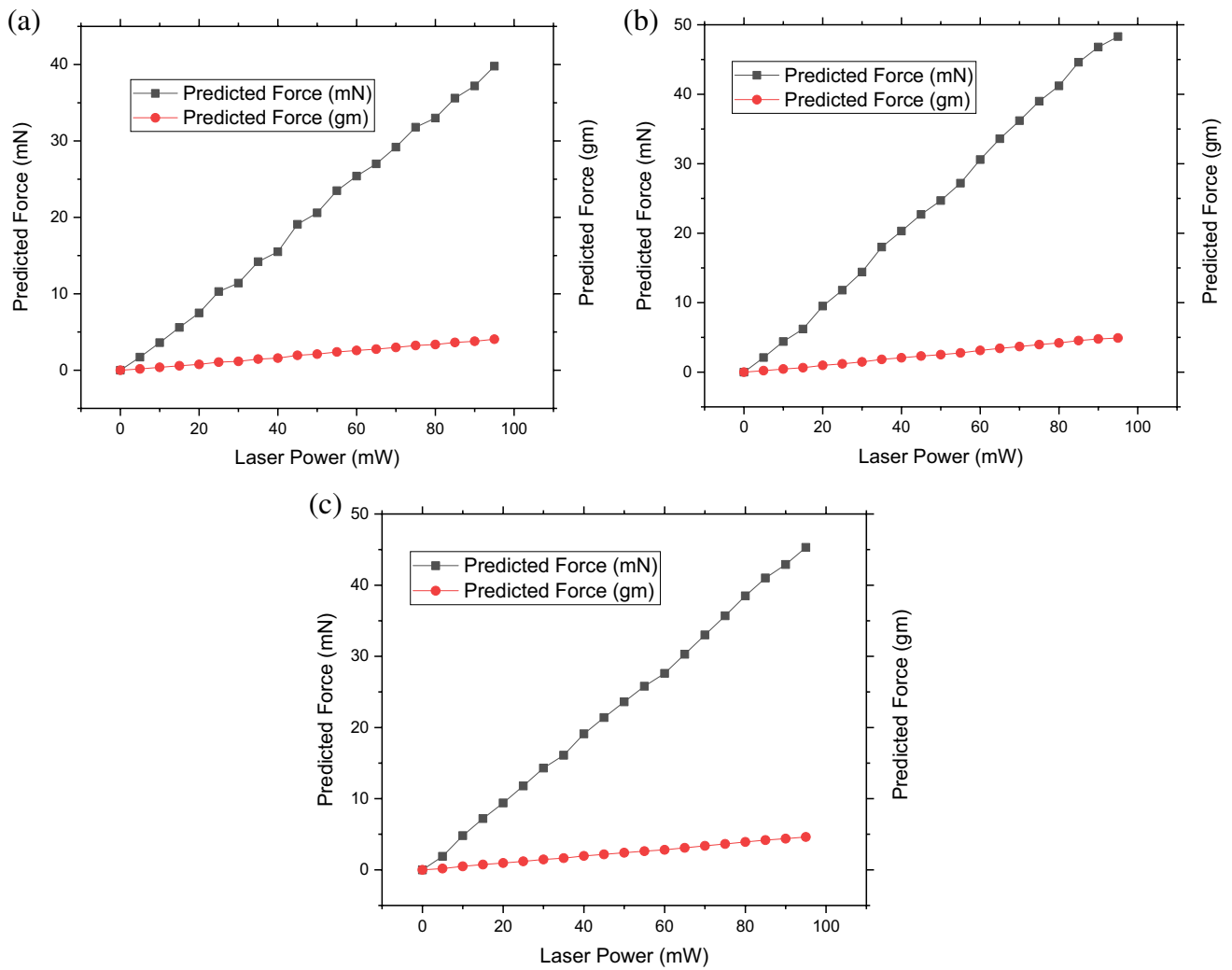
Fig. 12 a: Force exerted by red laser (655 nm). (**b**): Force exerted by blue laser (450 nm). (**c**): Force exerted by green laser (532 nm)

gripper end as mentioned in Table 3 above. The data is also presented in graphical form in Figs. 12(a-c) respectively.

Following Fig. 13(a) is the response curve created in ANSYS Response surface Methodology optimization process using design points as mentioned in Table 2. This response curve helps to determine optimized value

of force for a given vale of deflection of the gripper's holding-end.

Along with the response curve another curve, Fig. 13(b) has been represented below which is named as Goodness of Fit curve. This shows how the optimization process has taken care of the all the design points in the methodology.
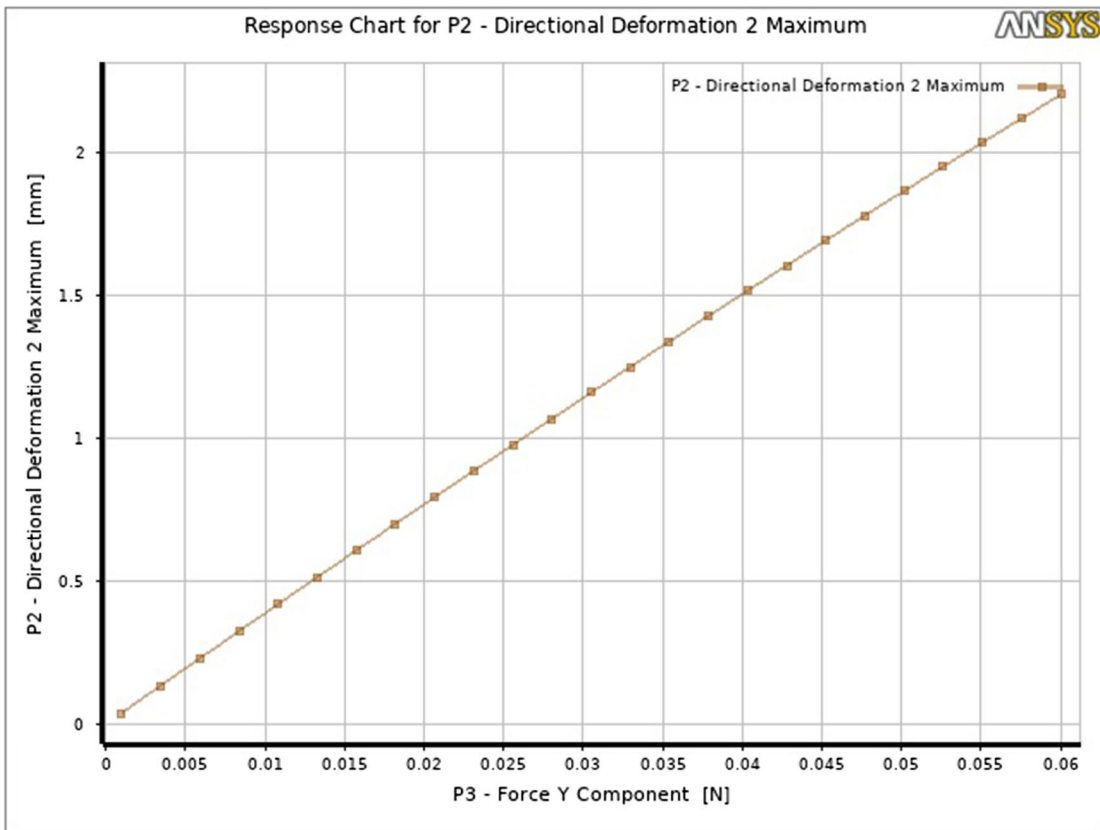
(a)
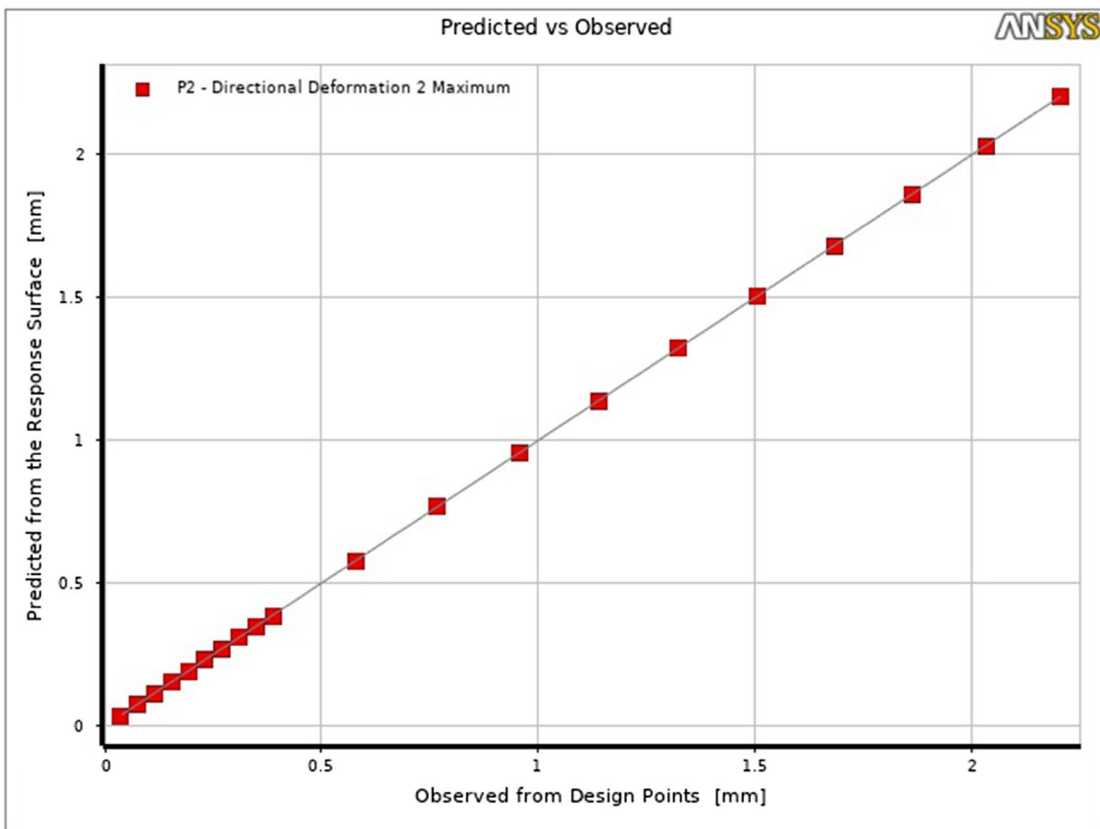
(b)

◀ **Fig. 13 a**: Response curve from all the design points created in the optimization. (**b**): Goodness of Fit for all the design points created in the optimization

Though there are many results have been derived in the process of optimization, results corresponding to the three lasers of highest wattage have been presented below in Figs. 14(a-c).

4 Conclusions

In the present work, numerical simulation using a FEA software named ANSYS has been used successfully to determine the force experienced by a FSMA strip attached between two aluminum arms of a micro gripper due to imposition of a given colored LASER beam of a given wattage value of energy at the concave portion of the FSMA strip. Here the force values have been evaluated by the method of 'Response Surface Optimization'. Force experienced by the FSMA strip also depends on the boundary condition imposed. The novelty of the work done in this work lies on the fact that this optimization model using a numerical software or more specifically a FEA software can predict the force which might be experienced by a FSMA Microgripper due to a specific laser under given boundary conditions. The data derived by this numerical optimization can be used for further experiment or analysis of the micro gripper.
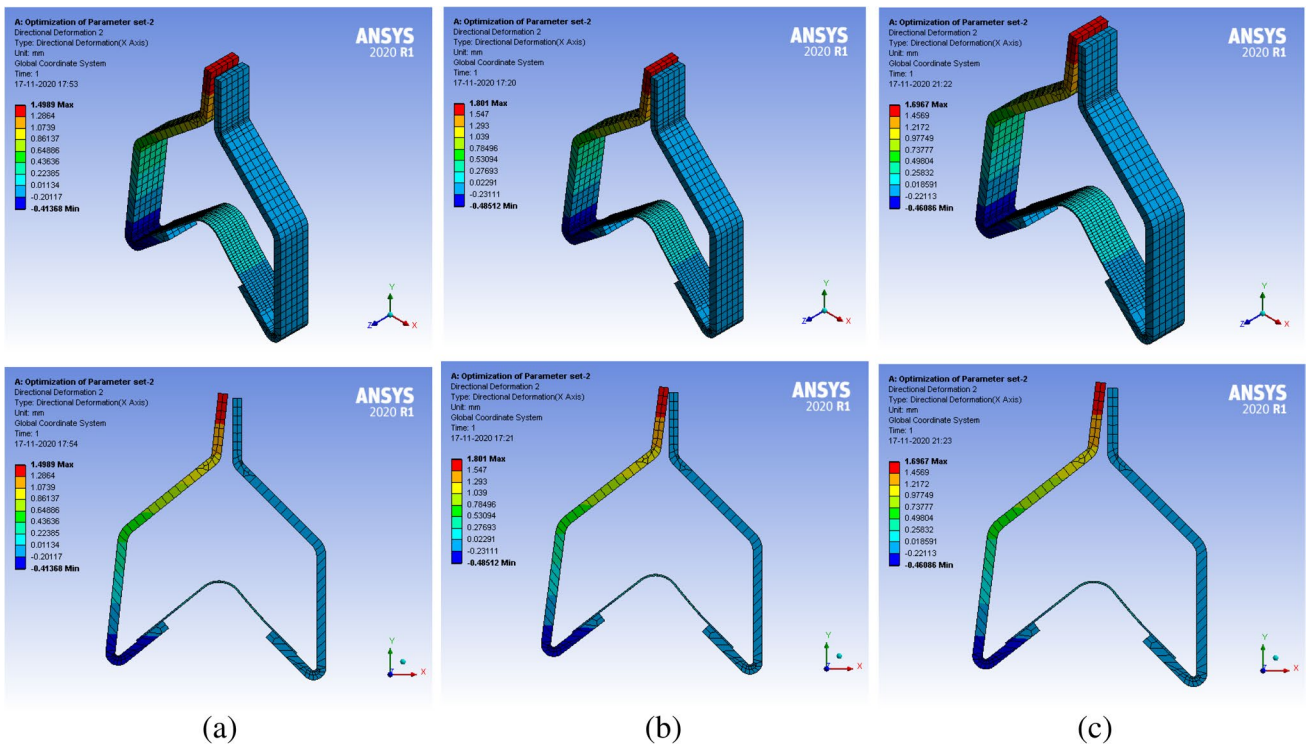

(a)   (b)   (c)

Fig. 14 a: Deflection of the gripper arm for red colored LASER with 95 mW power. (**b**): Deflection of the gripper arm for blue colored LASER with 95 mW power. (**c**): Deflection of the gripper arm for green colored LASER with 95 mW power

Data Availability The datasets generated during and/or analysed during the current study are available from the corresponding author on reasonable request.

Declarations

Conflicts of interests/Competing interests The authors have no competing interests to declare that are relevant to the content of this article.

References

1. Bryzek J (1996) Impact of MEMS technology on society. Sens. Actuators A Phys. 56:1
2. Judy JW (2001) Microelectromechanical systems (MEMS): fabrication, design and applications. Smart Mater. Struct. 10:1115
3. Nespoli A, Besseghini S, Pittaccio S, Villa E, Viscuso S (2010) The high potential of shape memory alloys in developing miniature mechanical devices: A review on shape memory alloy mini-actuators. Sens. Actuator A Phys. 158:149
4. Kohl M, Srinivasa Reddy Y, Khelfaoui F, Krevet B, Backen A, Fähler S, Eichhorn T, Jakob G, Mecklenburg A (2010) Recent Progress in FSMA Microactuator Developments. Mater. Sci. Forum 635:145
5. Kohl M, Krevet B, Ohtsuka M, Brugger D, Liu Y (2006) Ferromagnetic Shape Memory Microactuators. Mater. Trans. JIM 47:639
6. Kohl M, Gueltig M, Pinneker V, Yin R, Wendler F, Krevet B (2014) Magnetic Shape Memory Microactuators. Micromachines 5:1135
7. Lagoudas DC (ed) (2008) "Shape Memory Alloys Modeling and Engineering Applications" Springer
8. Murray SJ (2000) "Magneto-mechanical properties and applications of Ni-Mn-Ga ferromagnetic shape memory alloy", Ph. D thesis, Massachusetts Institute of Technology
9. Karaca HE, Karaman I, Basaran B, Ren Y, Chumlyakov YI, Maier HJ (2009) Magnetic Field-Induced Phase Transformation in NiMnCoIn Magnetic Shape Memory Alloys—A New Actuation Mechanism with Large Work Output. Adv. Funct. Mater. 19:983
10. Hu Z, Rajini Kanth B, Tamang R, Varghese B, Sow CH, Mukhopadhyay PK (2012) Visible microactuation of a ferromagnetic shape memory alloy by focused laser beam. Smart Mater. Struct. 21:032003
11. Bagchi A, Sarkar S, Mukhopadhyay PK (2018) Investigations on colour dependent photo induced microactuation effect of FSMA and proposing suitable mechanisms to control the effect. Indian J. Phys. 92:883
12. Bagchi A, Sarkar S, Bysakh S, Sarkar S, Mukhopadhyay PK (2019) Possible mechanisms for degradation of photo induced micro actuation effect in a ferromagnetic shape memory alloy at high temperatures. J. Appl. Phys. 125:144505
13. Bagchi A, Sarkar S, Bysakh S, Sarkar S, Mukhopadhyay PK (2020) Studies on the Effect of Temperature on the Photo-Induced Microactuation Effect of a Co-based FSMA System. Shap. Mem. Superelasticity 6:3
14. Alogla AF, Amalou F, Balmer C, Scanlan P, Shu W, Reuben RL (2015) Micro-tweezers: Design, fabrication, simulation and testing of a pneumatically actuated micro-gripper for micromanipulation and microtactile sensing. Sens. Actuator A Phys. 236:394
15. Jia Y, Xu Q (2013) MEMS Microgripper Actuators and Sensors: The State-of-the-Art Survey. Recent Pat. Mech. Engg. 6:132
16. Vargas-Chable P, Tecpoyotl-Torres M, Cabello-Ruiz R, Rodriguez-Ramirez JA, Vargas-Bernal R (2019) Modified U-shaped Microactuator with Compliant Mechanism Applied to a Microgripper. Actuators 8:28
17. Thangavel A, Rengaswamy R, Sukumar P (2019) Design and material analysis for prototyping of four arm mechanical microgripper with self-locking and anti-slipping capability. Microsyst. Technol. 25:851
18. Dechev N, Cleghorn WL, Mills JK (2003) Microassembly of 3-D MEMS Structures Utilizing a MEMS Microgripper with a Robotic Manipulator. IEEE International Conference on Robotics and Automation 3:3193
19. "Nikon Eclipse Ti-U inverted microscope" user manual.
20. Müllner P, Clark Z, Kenoyer L, Knowlton WB, Kostorz G (2008) Nanomechanics and magnetic structure of orthorhombic Ni-Mn-Ga martensite. Mater. Sci. Eng. A 481-482:66
21. Wu D, Crone WC, Perepezko J (2002) "Mechanical Behavior of Nanostructured Melt Spun NiTi Shape Memory Alloy", Society for Experimental Mechanics, 2002 SEM Annual Conference Proceedings, Milwaukee, WI
22. Jiang B, Wang J, Xu L, Qian C, Liu T, Dai J, Hou X (2018) Tunable Mechanical Properties of Ti-Zr-Ni-Cr-V Amorphous Ribbons via Different Melt Spinning Speeds during Rapid Solidification Process. Materials 11:947
23. Bagchi A, Sarkar S, Bysakh S, Tiwary CS, Hossain MS, Sarkar S, Mukhopadhyay PK (2020) Microstructural evolution and its outcome on the photo induced micro actuation effect and mechanical properties of copper doped Co-Ni-Al FSMA. J. Alloys Compd. 846:156432
24. Oliver W, Pharr G (1992) An improved technique for determining hardness and elastic modulus using load and displacement sensing indentation experiments. J Mater. Res. 7(6):1564

Publisher's Note Springer Nature remains neutral with regard to jurisdictional claims in published maps and institutional affiliations.